

longitudinally within the device. Measurements are carried out with a battery-supplied, constant a.c. sensing current of ≤ 500 nA; this is well below the onset of current-induced non-equilibrium effects. The induced transverse voltages are coupled through electrically isolated, low-noise differential amplifiers to a set of commonly synchronized lock-in amplifiers, which enable simultaneous acquisition of three signal channels. Both longitudinal and transverse resistances are recorded. The device is maintained at liquid helium temperature, while a magnetic field is applied within the epilayer plane via a precisely controlled, three-axis superconducting magnet. Magnetoresistance is obtained with a field oriented 15° away from [110] and ramped at a rate of 15 Oe s^{-1} .

Launching of individual DWs

We first apply a strong in-plane magnetic field to saturate the magnetization, then linearly ramp to a specific field magnitude with orientation anti-aligned to the initial saturation field (for example, close to the switching field labelled as point A in Fig. 1b). At ~ 4 K, DW nucleation then occurs infrequently through stochastic processes. Once nucleated, the constant in-plane field drives growth of the particular domain possessing magnetization most closely aligned with the applied field. We find that DW motion induced in this manner always involves propagation from a wide current contact pad into the channel. With this protocol, completely reproducible signals are detected.

High-resolution magnetoresistance measurements on single, stationary DWs

In the initial measurements, DWR was measured quasistatically as single DWs were sequentially driven slowly through the device. We have developed optimized techniques enabling high-resolution measurements on individual, stationary DWs. To accomplish this we have perfected a method allowing us to stepwise translate and position individual DWs along the device channel, through sequential, pulsed application of the in-plane magnetic field. Quick removal of the external field allows the DW to be 'frozen' at any desired location within the channel and, thereafter, the DW remains stationary for as long as we have been willing to measure. Subsequent application of in-plane field pulses allows the DW to be precisely stepped, in arbitrarily small increments, along the device channel. Between the applications of field pulses we are able to record longitudinal resistance across the stationary DW at zero applied field.

An individual DW is 'stepped' sequentially through the device, and its position is ascertained as follows. A magnetic field pulse—of magnitude 110 Oe, orientation 30° from hard axis [110], and duration 10 s—is applied every 8 min. For a given transverse-probe pair, a jump in transverse resistance is observed after each pulse, if the DW is proximal. Thereafter, the resistance remains unchanged until the next field pulse is applied. This giant planar Hall resistance allows direct computation of the DW's relative displacement from the transverse probes. Figure 4b displays the deduced positions of a DW when it is in the vicinity of the left and right pair of probes. This linear evolution of DW position confirms that the DW travels a constant, fixed distance in response to each field pulse—about $10 \mu\text{m}$ for the aforementioned conditions. For measurement points in the intermediate region, which may be 'far' from either transverse-probe pair, DW position can be reliably determined by linear extrapolation between known positions.

To enhance our ability to resolve the intrinsic DW resistivity, we minimize the longitudinal resistance background by precise alignment of the devices with respect to [110] orientation (to within $\sim 0.03^\circ$). This is achieved through a novel protocol based upon iterative, wafer-scale electron beam lithography (Fig. 3) that permits suppression of the AMR to a value as small as $\sim \Delta R/R = 6 \times 10^{-5}$. Two families of precisely aligned devices, with widths $30 \mu\text{m}$ and $60 \mu\text{m}$ and a constant 6:1 aspect ratio (that is, length/width) from a thinner (Ga,Mn)As epilayer (100 nm thickness, Curie temperature $T_C \approx 45$ K) have been iteratively patterned. The long 6:1 aspect ratio serves to extend the intermediate region that is unperturbed by eddy-like contributions (compare Fig. 2d). To preclude spurious DW trapping along the channel itself, transverse probes are located solely at the entrance and exit of each channel (Fig. 3c).

Received 3 April; accepted 2 July 2004; doi:10.1038/nature02809.

- Hubert, A. & Schäfer, R. *Magnetic Domains: The Analysis of Magnetic Microstructures* (Springer, Berlin, 1998).
- Ferré, J. Dynamics of magnetization reversal: From continuous to patterned ferromagnetic films. *Topics Appl. Phys.* **3**, 127–165 (2002).
- Berger, L. Low-field magnetoresistance and domain drag in ferromagnets. *J. Appl. Phys.* **49**, 2156–2161 (1978).
- Cabrera, G. G. & Falicov, L. M. Theory of residual resistivity of Bloch walls. *Phys. Status Solidi B* **61**, 539–549 (1974); **62**, 217–222 (1974).
- Viret, M. *et al.* Spin scattering in ferromagnetic thin films. *Phys. Rev. B* **53**, 8464–8468 (1996).
- Levy, P. M. & Zhang, S. Resistivity due to domain wall scattering. *Phys. Rev. Lett.* **79**, 5110–5113 (1997).
- Tatara, G. & Fukumura, H. Resistivity due to a domain wall in ferromagnetic metal. *Phys. Rev. Lett.* **78**, 3773–3776 (1997).
- van Gorkom, R. P., Brataas, A. & Bauer, G. E. W. Negative domain wall resistance in ferromagnets. *Phys. Rev. Lett.* **83**, 4401–4404 (1999).
- Viret, M. *et al.* Anisotropy of domain wall resistance. *Phys. Rev. Lett.* **85**, 3962–3965 (2000).
- Ruediger, U., Yu, J., Zhang, S., Kent, A. D. & Parkin, S. S. P. Negative domain wall contribution to the resistivity of microfabricated Fe wires. *Phys. Rev. Lett.* **80**, 5639–5642 (1998).
- Klein, L. *et al.* Domain wall resistivity in SrRuO₃. *Phys. Rev. Lett.* **84**, 6090–6093 (2000).
- Ebels, U., Radulescu, A., Henry, Y., Piroux, L. & Ounadjela, K. Spin accumulation and domain wall magnetoresistance in 35 nm Co wires. *Phys. Rev. Lett.* **84**, 983–986 (2000).
- Taniyama, T., Nakatani, L., Namikawa, T. & Yamazaki, Y. Resistivity due to domain walls in Co zigzag wires. *Phys. Rev. Lett.* **82**, 2780–2783 (1999).
- Xu, Y. B. *et al.* Magnetoresistance of a domain wall at a submicron junction. *Phys. Rev. B* **61**, R14901–R14904 (2000).
- Danneau, R. *et al.* Individual domain wall resistance in submicron ferromagnetic structures. *Phys. Rev. Lett.* **88**, 157201–157204 (2002).

- Allwood, D. A. *et al.* Submicrometer ferromagnetic NOT gate and shift register. *Science* **296**, 2003–2006 (2002).
- Ono, T. *et al.* Propagation of a magnetic domain wall in a submicrometer magnetic wire. *Science* **284**, 468–470 (1999).
- Wolf, S. A. *et al.* Spintronics: A spin-based electronics vision for the future. *Science* **294**, 1488–1495 (2001).
- Tang, H. X., Kawakami, R. K., Awschalom, D. D. & Roukes, M. L. Giant planar Hall effect in epitaxial (Ga,Mn)As devices. *Phys. Rev. Lett.* **90**, 107201–107204 (2003).
- Ohno, H. Making nonmagnetic semiconductors ferromagnetic. *Science* **281**, 951–956 (1998).
- Yamanouchi, M., Chiba, D., Matsukura, F. & Ohno, H. Current-induced domain-wall switching in a ferromagnetic semiconductor structure. *Nature* **428**, 539–542 (2004).
- Welp, U., Vlasko-Vlasov, V. K., Liu, X., Furdyna, J. K. & Wojtowicz, T. Magnetic domain structure and magnetic anisotropy in Ga_{1-x}MnAs. *Phys. Rev. Lett.* **90**, 167206–167209 (2003).
- Tang, H. X., Kawakami, R. K., Awschalom, D. D., Roukes, M. L. *Phys. Rev. Lett.* (submitted).
- Tang, H. X. & Roukes, M. L. Electrical transport across an individual magnetic domain wall in (Ga,Mn)As microdevices. *Phys. Rev. B* (submitted); preprint at (<http://arxiv.org/cond-mat/0403547>) (2004).
- Potashnik, S. J. *et al.* Saturated ferromagnetism and magnetization deficit in optimally annealed Ga_{1-x}MnAs epilayers. *Phys. Rev. B* **66**, 012408 (2002).
- Tang, H. X. *Semiconductor Magnetoelectronics for Spintronics and Suspended 2DEG for Mechanoelectronics* PhD dissertation, California Inst. Technol. (2002).

Acknowledgements We acknowledge support from DARPA/DSO and AFOSR. We thank A.H. MacDonald for discussions.

Competing interests statement The authors declare that they have no competing financial interests.

Correspondence and requests for materials should be addressed to M.L.R. (roukes@caltech.edu).

Decline of surface temperature and salinity in the western tropical Pacific Ocean in the Holocene epoch

Lowell Stott¹, Kevin Cannariato¹, Robert Thunell², Gerald H. Haug³, Athanasios Koutavas⁴ & Steve Lund¹

¹Department of Earth Sciences, University of Southern California, Los Angeles, California 90089, USA

²Department of Geological Sciences, University of South Carolina, Columbia, South Carolina 29205, USA

³Geforsschungszentrum Potsdam, D-14473 Potsdam, Germany

⁴Department of Earth, Atmospheric, and Planetary Sciences, Massachusetts Institute of Technology, 77 Massachusetts Avenue, Cambridge, Massachusetts 02139, USA

In the present-day climate, surface water salinities are low in the western tropical Pacific Ocean and increase towards the eastern part of the basin¹. The salinity of surface waters in the tropical Pacific Ocean is thought to be controlled by a combination of atmospheric convection, precipitation, evaporation and ocean dynamics², and on interannual timescales significant variability is associated with the El Niño/Southern Oscillation cycles. However, little is known about the variability of the coupled ocean-atmosphere system on timescales of centuries to millennia. Here we combine oxygen isotope and Mg/Ca data from foraminifers retrieved from three sediment cores in the western tropical Pacific Ocean to reconstruct Holocene sea surface temperatures and salinities in the region. We find a decrease in sea surface temperatures of $\sim 0.5^\circ\text{C}$ over the past 10,000 yr, whereas sea surface salinities decreased by ~ 1.5 practical salinity units. Our data imply either that the Pacific basin as a whole has become progressively less salty or that the present salinity gradient along the Equator has developed relatively recently.

On interannual timescales, the El Niño/Southern Oscillation (ENSO) causes large changes in salinity over the equatorial Pacific as the warm, low-salinity waters from the western tropical

Pacific (WTP) are advected east into the central Pacific. This redistribution of warm waters along the Equator also alters the locus of atmospheric convection and seems to enhance the transport of heat from the tropics to higher latitudes²⁻⁴. On longer timescales it is possible that other modes of variability have existed that can only be ascertained through analysis of long proxy records.

We reconstructed WTP sea surface temperature (SST) and the stable oxygen isotope composition of surface water ($\delta^{18}\text{O}_{\text{SW}}$) variability through the Holocene as a method of determining how the freshwater flux and ocean dynamics varied in the past and how that variability affected salinity gradients in the tropics. In the WTP, sea surface salinity (SSS) and $\delta^{18}\text{O}_{\text{SW}}$ are correlated, reflecting the balance between the freshwater flux (evaporation – precipitation) and salt advection by means of ocean transport. A change in the $\delta^{18}\text{O}$ of fresh water or the amount of fresh water falling on the ocean relative to inputs of salty water by means of ocean dynamics changes the salinity and also $\delta^{18}\text{O}_{\text{SW}}$. Groundwater $\delta^{18}\text{O}$ values of early, middle and late Holocene age from sites in the WTP all have the same value as present-day monsoon rainwater, indicating there has not been a change in the isotopic value of fresh water falling on the ocean over this period⁵. We therefore expect WTP $\delta^{18}\text{O}_{\text{SW}}$ values to have been controlled during the Holocene primarily by the combined effects of changing freshwater flux (the amount effect) and the flux of salty water through the WTP by means of ocean dynamics. Today these two processes result in a surface water $\delta^{18}\text{O}$ /salinity relationship that has a slope of between 0.3‰ and 0.4‰ per practical salinity unit (p.s.u.)^{6,7}.

The $\delta^{18}\text{O}_{\text{SW}}$ is incorporated into CaCO_3 shells of planktonic foraminifers that inhabit the surface ocean. To reconstruct past changes in $\delta^{18}\text{O}_{\text{SW}}$ we analysed the stable oxygen isotopic composition and Mg/Ca of calcium carbonate produced by the

surface-dwelling planktonic foraminifer *Globigerinoides ruber*. The carbonate shells of this foraminifer accumulated on the sea floor throughout the Holocene and became part of the sediment archive that was cored by the IMAGES programme in 1998 (Fig. 1). Using foraminiferal samples from three WTP IMAGES cores we reconstructed a continuous record of sea surface temperatures with Mg/Ca palaeothermometry⁸, which has an estimated uncertainty of $\pm 1^\circ\text{C}$. We also measured the $\delta^{18}\text{O}_{\text{C}}$ of the same foraminiferal material. The isotopic measurements have an analytical precision of $\pm 0.1\text{‰}$ and a practical sample reproducibility of about $\pm 0.1\text{‰}$. Combining the temperature estimates with the measured values of *G. ruber* $\delta^{18}\text{O}_{\text{C}}$, we derived values of $\delta^{18}\text{O}_{\text{SW}}$ from the carbonate palaeotemperature equation (Supplementary Information).

Our measurements are combined with previously published data from equatorial Pacific ODP Site 806 (ref. 9) to examine how surface water properties in the WTP between Indonesia and the open Pacific have varied through the Holocene epoch (Fig. 1). Samples from the Indonesian sites provide a multidecadal (MD81 and MD76) to centennial (MD70) temporal resolution through the entire Holocene, whereas the open-ocean ODP Site 806 record is of millennial resolution. Other high-quality late Pleistocene and early Holocene records are available from the Sulu Sea¹⁰ but do not provide a continuous record through the entire Holocene. The sites discussed here are all located between 6°N and 11°S (Fig. 1) and the chronology for each core is based on radiocarbon dating of fossil carbonates.

Between 10 kyr ago and the late Holocene, the $\delta^{18}\text{O}$ of *G. ruber* ($\delta^{18}\text{O}_{\text{C}}$) at each of the WTP sites decreased by $\sim 0.4\text{‰}$ (Fig. 1). Because this trend occurred after Northern Hemisphere ice sheets had mostly retreated, a change in ice volume cannot account for the

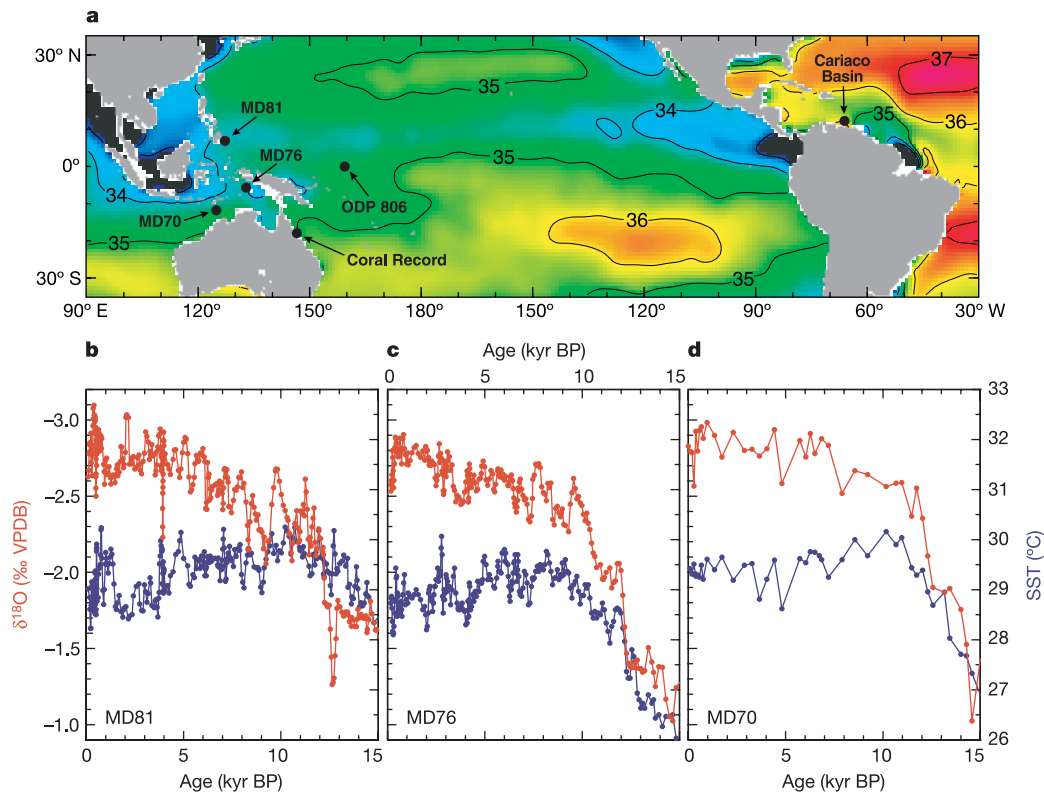


Figure 1 Western tropical Pacific marine sediment core locations and corresponding climate records. **a**, Map of mean annual surface salinities in the tropical Pacific¹ illustrating the location of IMAGES MD core locations from which the oxygen isotope (red

in **b-d**) and Mg/Ca–palaeoSST records (blue in **b-d**) were generated for this study. **b-d**, Results from individual sites: **b**, MD81; **c**, MD76; **d**, MD70. The data from sites MD81 and MD76 have been smoothed with a 3-point running mean.

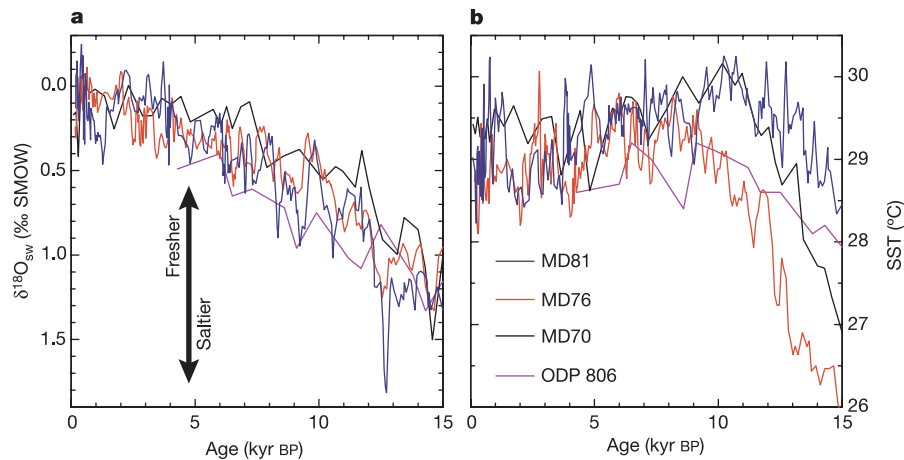


Figure 2 Reconstructed records for WTP sites. **a**, $\delta^{18}\text{O}_{\text{SW}}$; **b**, SST. The $\delta^{18}\text{O}_{\text{SW}}$ values were calculated by solving the calcite palaeotemperature equation for $\delta^{18}\text{O}_{\text{SW}}$ using the

foraminiferal Mg/Ca temperatures and the $\delta^{18}\text{O}$ values. Blue, MD81; red, MD76; black, MD70; purple, ODP 806.

large change in $\delta^{18}\text{O}_{\text{C}}$ during the late Holocene¹¹. The trend in $\delta^{18}\text{O}_{\text{C}}$ must reflect either SST warming through the Holocene, which produces a smaller isotope fractionation and lower $\delta^{18}\text{O}$ values in calcium carbonate, or a decrease in the local $^{18}\text{O}/^{16}\text{O}$ of surface waters. The Mg/Ca-derived SSTs constrain how much of the $\delta^{18}\text{O}$ trend can be attributed to temperature change. Our SST estimates indicate that surface waters across the WTP were warmest in the early Holocene ($\sim 29.5^\circ\text{C}$) and have cooled by $\sim 0.5^\circ\text{C}$ since 10 kyr ago (Fig. 2). This seems to be a robust feature of each of the records between 6°N and 11°S and is therefore unlikely to be solely a result of summer isolation changes associated with the precessional cycle. Changes in cloud albedo, evaporation and ocean dynamics arising from the precessional forcing might have contributed to the change in SST¹². But on the basis of these data alone, we cannot ascertain how these factors combined to cause the higher temperatures during the early Holocene. Nonetheless, the trend in SST does not explain the decreasing foraminiferal $\delta^{18}\text{O}_{\text{C}}$ values between the middle to late Holocene. This trend must reflect a change in the $\delta^{18}\text{O}_{\text{SW}}$ and surface salinity during the Holocene. To estimate the magnitude of the salinity change since the early Holocene we stacked the WTP $\delta^{18}\text{O}_{\text{C}}$ and Mg/Ca records, averaging the data at 250-yr intervals. The stacked data were then used to calculate $\delta^{18}\text{O}_{\text{SW}}$. Since ~ 8 kyr ago, $\delta^{18}\text{O}_{\text{SW}}$ values have decreased in the WTP by 0.5‰ (Fig. 3). On the basis of the modern $\delta^{18}\text{O}$ –salinity relationship^{6,7}, a decrease in $\delta^{18}\text{O}_{\text{SW}}$ of 0.5‰ reflects a decrease in surface salinity of between 1 and 1.5 p.s.u. This observation implies that in the early Holocene WTP surface water was as salty as surface water in the south central equatorial Pacific today (more than 35.2 p.s.u.). This observation further implies that if the salinities in the central and eastern equatorial Pacific have not changed in association with those in the WTP, the salinity gradient that exists today across the tropical Pacific would have been absent or significantly reduced in the early to middle Holocene.

Higher $\delta^{18}\text{O}_{\text{SW}}$ values have also been recognized in a middle Holocene coral record from the Great Barrier reef¹³, indicating these higher salinities extended over large portions of the WTP (Fig. 1). The higher $\delta^{18}\text{O}_{\text{SW}}$ values from the Great Barrier Reef were interpreted to reflect enhanced evaporation over that portion of the WTP during the middle Holocene. We find it difficult to reconcile the higher $\delta^{18}\text{O}_{\text{SW}}$ values that we observe in the early to middle Holocene in the northern WTP with increased evaporation because the surface salinities in this region are so strongly influenced by summer monsoon precipitation, which most climate models indi-

cate would have been enhanced in the middle Holocene by increased solar heating in boreal summer associated with the precessional forcing¹⁴. Today, the northern WTP receives in excess of 2 m of rainfall during the summer monsoon. The isotopic composition of this water is about -6.5‰ . Groundwater of early to late Holocene age from the Philippines has the same $\delta^{18}\text{O}_{\text{SMOW}}$ as modern rainwater, indicating that the source of moisture to the region has not changed during the Holocene⁵. Therefore, if the isotopic composition of rain has not changed, an isotope mass balance calculation (with no change in ocean transport) would require there to have been a decrease in rainfall of more than 2 m (the entire seasonal rainfall amount today) to shift a 25-m-thick ocean mixed layer by the observed 0.5‰ . There is no evidence for such a drastic decrease in monsoon rainfall during the Holocene. In fact, the early to middle Holocene groundwater $\delta^{18}\text{O}_{\text{SMOW}}$ values imply that there has been a persistent and strong monsoon system throughout the Holocene¹. We conclude that the increased $\delta^{18}\text{O}_{\text{SW}}$ values in the early Holocene were not due to increased evaporation but rather were the result of either increased westward advection of salty waters through the WTP, which would imply very different salinity gradients along the Equator compared with today or that the Pacific surface waters as a whole have become progressively less salty.

With only a limited number of high-resolution Holocene $\delta^{18}\text{O}_{\text{SW}}$ records available from other parts of the global ocean it is not

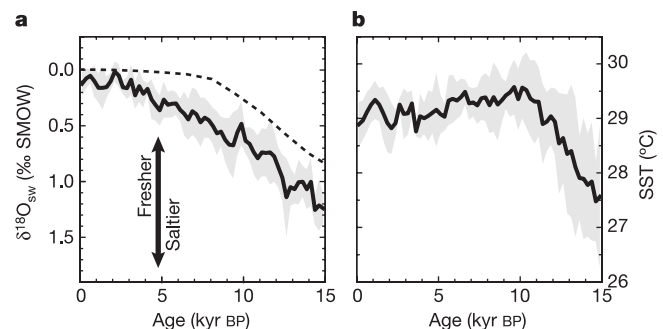


Figure 3 Stacked (average value) **(a)** $\delta^{18}\text{O}_{\text{SW}}$ and **(b)** SST records from Fig. 2, with 1σ uncertainty envelope (grey). Dashed line in panel **a** is the $\delta^{18}\text{O}_{\text{SW}}$ change due to the melting ice sheets reconstructed from stacked benthic foraminiferal $\delta^{18}\text{O}$ records¹⁹.

possible to assess whether the observed changes in the WTP reflect a larger, basin-scale change in the isotopic composition of the ocean. However, numerical model simulations have suggested that sustained shifts in the location of the Intertropical Convergence Zone (ITCZ) over the tropical Atlantic Ocean would probably affect the vapour flux to the Pacific, and change the fresh water as well as the isotopic balance over the oceans¹⁵. A persistent displacement of the ITCZ to more northerly latitudes in summer would act to trap isotopically light vapour within the Atlantic basin and decrease the vapour gain in the Pacific. The salinity and $\delta^{18}\text{O}$ changes we document from the WTP occurred in close association with the precessional cycle and with enhanced solar heating in the northern tropics during the early Holocene, which would have tended to pull the ITCZ north off its present summer latitude¹⁴. Over the course of millennia a northerly bias in the latitude of the ITCZ and reduced vapour transport between the oceans could have affected the isotopic composition of Pacific surface waters. At present there are no continuous SSS records from the tropical Atlantic and eastern Pacific that span the entire Holocene and provide the same temporal resolution that is available for the WTP. Nonetheless, previous studies have documented an early Holocene pluvial over North Africa and a stronger Indian Ocean summer monsoon in response to Earth's precessional cycle^{16,17}. Cariaco Basin sediments also contain evidence of higher rainfall in northern South America during the early Holocene, with increasingly arid conditions developing during the past 5,000 yr (ref. 18). These data all point to tropic-wide changes in the hydrological cycle that have been attributed to a more northerly position of the ITCZ during the early Holocene in response to changes in solar radiation associated with the precessional cycle. Data from other parts of the Pacific and Atlantic will now be required for an assessment of whether the changes in the hydrologic cycle affected the salinity gradient between the Pacific and Atlantic Oceans. If so, millennial to centennial scale changes in Holocene ocean thermohaline circulation would be directly affected by ocean-atmosphere processes that have occurred in the tropics. □

Received 22 January; accepted 26 July 2004; doi:10.1038/nature02903.

- Levitus, S. & Boyer, T. P. *World Ocean Atlas 1994* Vol. 3, *Salinity* (NOAA Atlas NESDIS, US Department of Commerce, Washington DC, 1994).
- Cronin, M. F. & McPhaden, M. J. Upper ocean salinity balance in the western equatorial Pacific. *J. Geophys. Res.* **103**, 27567–27587 (1998).
- Sun, D.-Z. & Trenberth, K. E. Coordinated heat removal from the equatorial Pacific during the 1986–87 El Niño. *Geophys. Res. Lett.* **25**, 2659–2662 (1998).
- McPhaden, M. J. Genesis and evolution of the 1997–98 El Niño. *Science* **283**, 950–954 (1999).
- Aggarwal, P. K., Fröhlich, K., Kulkarni, K. M. & Gourcy, L. L. Stable isotope evidence for moisture sources in the Asian summer monsoon under present and past climate regimes. *Geophys. Res. Lett.* **31**, doi:10.1029/2004GL019911 (2004).
- Fairbanks, R. G. *et al.* Evaluating climate indices and their geochemical proxies measured in corals. *Coral Reefs* **16**, S93–S100 (1997).
- Morimoto, M. *et al.* Salinity records for the 1997–98 El Niño from Western Pacific corals. *Geophys. Res. Lett.* **29**, doi:10.1029/2001GL013521 (2002).
- Nürnberg, D., Bijma, J. & Hemleben, C. Assessing the reliability of magnesium in foraminiferal calcite as a proxy of water mass temperature. *Geochim. Cosmochim. Acta* **60**, 803–814 (1996).
- Lea, D. W., Pak, D. K. & Spero, H. J. Climate impact of late Quaternary equatorial Pacific sea surface temperature variations. *Science* **289**, 1719–1724 (2000).
- Oppo, D. W., Linsley, B. K., Rosenthal, Y., Dannenmann, S. & Beaufort, L. Orbital and suborbital climate variability in the Sulu Sea, western tropical Pacific. *Geochim. Geophys. Geosyst.* **4**, doi:10.1029/2001GC000260 (2003).
- Fairbanks, R. A 17,000-year glacio-eustatic sea level record: influence of glacial melting rates on the Younger Dryas event and deep-ocean circulation. *Nature* **342**, 637–642 (1989).
- Clement, A. C., Seager, R. & Cane, M. A. Orbital controls on the El Niño/Southern Oscillation and the tropical climate. *Paleoceanography* **14**, 441–456 (1999).
- Gagan, M. K. *et al.* Temperature and surface-ocean water balance of the mid-Holocene tropical western Pacific. *Science* **279**, 1014–1018 (1998).
- Liu, Z., Kutzbach, J. & Wu, L. Modeling climate shift of El Niño variability in the Holocene. *Geophys. Res. Lett.* **27**, 2265–2268 (2000).
- Schmittner, A., Appenzeller, Z. & Stocker, T. F. Enhanced Atlantic freshwater export during El Niño. *Geophys. Res. Lett.* **27**, 1163–1166 (2000).
- Prell, W. L. & Van Campo, E. Coherent response of Arabian Sea upwelling and pollen transport to late Quaternary monsoonal winds. *Nature* **323**, 526–528 (1986).
- DeMenocal, P., Ortiz, J., Guilderson, T. & Sarnthein, M. Coherent high- and low-latitude climate variability during the Holocene warm period. *Science* **288**, 2198–2202 (2000).
- Haug, G. H. *et al.* Southward migration of the Intertropical Convergence Zone through the Holocene. *Science* **293**, 1304–1308 (2001).

- Waelbroeck, C. *et al.* Sea-level and deep water temperature changes derived from benthic foraminifera isotopic records. *Quat. Sci. Rev.* **21**, 295–305 (2002).

Supplementary Information accompanies the paper on www.nature.com/nature.

Acknowledgements We thank M. Rincon for analytical assistance. This research was supported by the US-NSF-OCE.

Competing interests statement The authors declare that they have no competing financial interests.

Correspondence and requests for materials should be addressed to L.S. (stott@usc.edu). The foraminiferal $\delta^{18}\text{O}$ and Mg/Ca data are available at <http://www.ngdc.noaa.gov>.

Osmium isotopic constraints on the nature of the DUPAL anomaly from Indian mid-ocean-ridge basalts

S. Escrig¹, F. Capmas¹, B. Dupré² & C. J. Allègre¹

¹Laboratoire de Géochimie et Cosmochimie (UMR 7579 CNRS), Institut de Physique du Globe de Paris, Université Denis Diderot (Paris 7), 4 place Jussieu, 75252 Paris Cedex 05, France

²Laboratoire des Mécanismes et Transfert en Géologie (UMR 5563 CNRS), Université Paul Sabatier, 38 rue des Trente-Six Ponts, 31400 Toulouse, France

The isotopic compositions of mid-ocean-ridge basalts (MORB) from the Indian Ocean have led to the identification of a large-scale isotopic anomaly relative to Pacific and Atlantic ocean MORB¹. Constraining the origin of this so-called DUPAL anomaly² may lead to a better understanding of the genesis of upper-mantle heterogeneity. Previous isotopic studies^{3–10} have proposed recycling of ancient subcontinental lithospheric mantle or sediments with oceanic crust to be responsible for the DUPAL signature. Here we report Os, Pb, Sr and Nd isotopic compositions of Indian MORB from the Central Indian ridge, the Rodriguez triple junction and the South West Indian ridge. All measured samples have higher ¹⁸⁷Os/¹⁸⁸Os ratios than the depleted upper-mantle value^{11,12} and Pb, Sr and Nd isotopic compositions that imply the involvement of at least two distinct enriched components in the Indian upper-mantle. Using isotopic and geodynamical arguments, we reject both subcontinental lithospheric mantle and recycled sediments with oceanic crust as the cause of the DUPAL anomaly. Instead, we argue that delamination of lower continental crust may explain the DUPAL isotopic signature of Indian MORB.

In the Pb–Sr–Nd isotopic space, the Indian MORB array differs from the Pacific and Atlantic arrays by a distinct ‘low ²⁰⁶Pb/²⁰⁴Pb’ end-member characterized by lower ²⁰⁶Pb/²⁰⁴Pb, ¹⁴³Nd/¹⁴⁴Nd and higher ²⁰⁷Pb/²⁰⁴Pb, ²⁰⁸Pb/²⁰⁴Pb and ⁸⁷Sr/⁸⁶Sr ratios. These compositions imply the presence in the upper Indian mantle of a component that has undergone a long time-integrated evolution with high Th/U, Rb/Sr ratios and low U/Pb, Sm/Nd ratios relative to the Atlantic–Pacific upper mantle. Previous Sr–Nd–Pb isotopic studies^{3–10} of Indian MORB have related the DUPAL signature to recycled continental lithosphere, either as old subcontinental lithosphere or as sediments associated with oceanic crust. Subcontinental lithosphere requires the presence in the upper mantle of another recycled component having HIMU-like isotopic compositions (that is, high $\mu = ^{238}\text{U}/^{204}\text{Pb}$) whereas recycled oceanic crust associated with variable amounts of sediments may produce both the HIMU